Erciyes Üniversitesi
Fen Bilimleri Enstitüsü Dergisi
Cilt 40, Sayı 2 , 2024

Erciyes University
Journal of Institue Of Science and Technology
Volume 40, Issue 2, 2024

Determination of Johnson Cook Strength and Failure Parameters of EN-GJS-400 Spheroidal Graphite Cast Iron

Burak Özcan*[1] , Ulvi Şeker[2],

*[1] Gazi University, Graduate School of Natural and Applied Sciences, ANKARA
[2] Gazi University, Faculty of Technology, Department of Manufacturing Engineering, ANKARA

(Alınış / Received: 25.07.2024, Kabul / Accepted: 19.08.2024, Online Yayınlanma / Published Online: 30.08.2024)

Keywords
EN-GJS-400,
Johnson-Cook,
Split Hopkinson,
Finite Element Analysis

Abstract: In this study, to investigate the mechanical behavior of EN-GJS-400 nodular cast iron material, quasi-static tensile tests were conducted at room temperature and at 300°C, 500°C, and 700°C, along with compression tests at room temperature. To examine the behavior at high deformation rates, Split Hopkinson tests were carried out at four different strain rates, reaching up to approximately 4500/s. To reveal the damage behavior of the materials, tensile tests were conducted with four different notches (R=1.25, 2.5, 5, 10mm). Microstructure experiments and spectral analyses of the materials were performed. Based on the data obtained from the experiments, Johnson-Cook (J-C) material and damage model parameters were calculated. The calculated J-C material and damage parameters were defined in the Abaqus finite element software, and virtual tensile tests were conducted and compared with the actual test data. The actual test data and the tests performed in the computer environment were similar to each other.

EN-GJS-400 Küresel Grafitli Dökme Demir Malzemenin Johnson Cook Malzeme ve Hasar Parametrelerinin Belirlenmesi

Anahtar Kelimeler
EN-GJS-400,
Johnson-Cook,
Split Hopkinson
Sonlu Elemanlar Analizi

Öz: Bu çalışma kapsamında EN-GJS-400 küresel grafitli dökme demir malzemenin mekanik davranışlarını incelemek için oda koşullarında ve 300, 500 ve 700° derece sıcaklıklarda yarı statik çekme ve oda koşullarında basma deneyleri gerçekleştirilmiştir. Yüksek şekil değiştirme hızlarında davranışlarını incelemek için dört farklı şekil değiştirme hızında yaklaşık, maksimum 5500/s gerinim hızına kadar Split Hopkinson testleri gerçekleştirilmiştir. Malzemelerin hasar davranışlarını ortaya koyabilmek için 4 farklı çentikte (R=1.25, 2.5, 5, 10mm) çekme deneyleri gerçekleştirilmiştir. Malzemelerin mikro yapı deneyleri ve spektral analizleri gerçekleştirilmiştir. Deneylerde elde edilen veriler doğrultusunda Johnson-Cook(J-C) malzeme ve hasar model parametreleri hesaplanmıştır. Hesaplanan JC malzeme ve hasar parametreleri Abaqus sonlu elemanlar yazılımında tanımlanarak çekme testleri sanal ortamda gerçekleştirilmiş ve gerçek test verileriyle karşılaştırılmıştır. Gerçek test veriyle bilgisayar ortamanında gerçekleştirilen testler birbirleriyle benzerlik göstermiştir.

*İlgili Yazar, email: ozcan.burak@outlook.com

1. Introduction

Ram and Gautam (2022)[1] focuses on developing the Johnson-Cook (J-C) material model parameters for Si-Mo-Cr ductile cast iron, which is a promising material for automotive, defense, and aeronautical applications due to its high tensile strength, fracture toughness, and wear resistance. The researchers prepared Si-Mo-Cr ductile cast iron by controlled melting and magnesium treatment, followed by uniaxial tensile tests conducted at different strain rates and temperatures. The study revealed that the material exhibits positive strain rate dependency and that its tensile strength increases with strain rate, while ductility decreases. The J-C parameters, including yield strength (A), strain hardening constant (B), strain hardening exponent (n), strain rate sensitivity coefficient (C), and thermal softening coefficient (m), were determined using standard equations. The findings indicate that the microstructural characteristics, such as nodularity and pearlite content, significantly influence the material's mechanical properties and its performance under varying strain rates and temperatures.

Hellström and Olander (2015)[2] focused on the characterization and modeling of Compacted Graphite Iron (CGI) at a microstructural level using the Johnson-Cook (JC) material model. The study aimed to obtain material parameters that accurately represent the deformation and fracture behavior of CGI, particularly in machining processes. The researchers conducted tensile tests on CGI specimens with various notch geometries and used Digital Image Correlation (DIC) to capture strain fields during testing. Finite Element Analysis (FEA) was employed to calculate stress triaxiality in the fracture zones. The obtained material parameters were optimized using MATLAB to fit the JC hardening and fracture models. The study compared a homogeneous approach, treating CGI as a single-phase material, with a heterogeneous approach that accounts for the distinct phases of pearlite and graphite within CGI. The results indicated that while the JC model is effective, it has limitations in capturing certain fracture behaviors, suggesting the need for further investigation and validation of the parameters obtained.

Ljustina, Larsson, and Fagerström (2014)[3] developed a finite element (FE) based simulation methodology to account for the microstructural characteristics of cast iron, particularly focusing on graphite nodularity and its impact on machinability. The study integrates detailed microstructural data obtained from micrograph images into the FE model, allowing for accurate representation of pearlite and graphite phases within the cast iron. The Johnson-Cook viscoplasticity model was utilized to describe the continuous deformation behavior, and a fracture model was applied to simulate chip formation during machining. The researchers conducted a parametric study to investigate how varying degrees of graphite nodularity affect cutting forces and temperatures. The findings show that the model successfully predicts the influence of microstructure on machinability, with simulations correlating well with experimental results, particularly in terms of cutting force and chip formation

Keser (2015)[4] calculated the parameters of the Johnson-Cook material model for GJV material and developed the material model through experimental and analytical methods. Data from quasi-static tensile tests conducted at 20°C, 300°C, 400°C, 500°C, and 700°C were used, and SHPB test specimens were prepared to obtain values at high strain rates. Tests were performed at strain rates of 1530, 1550, 2000, and 2200 s-1, and the parameters A, B, C, n, and m were determined. These parameters were made ready for use in orthogonal cutting simulations with SEY, allowing the effects of plastic deformation, strain rate, and temperature changes on stress to be seen in a formula. After determining the A parameter, which corresponds to yield strength, from the tensile test conducted at 200°C and quasi-static conditions, the B and n parameters were also found using the same data. The C parameter was then obtained from the SHPB test conducted at high deformation rates, and finally, the m parameter was derived from static tests conducted at different temperatures. To further improve the results, a compression test was performed at a deformation rate of 1 s-1, and the obtained parameters were refined. The mechanical properties of the material were compared with the Johnson-Cook parameters of Gray Cast Iron and Spheroidal Graphite Cast Iron

Springer (2012)[5] conducted a comprehensive study to characterize the strength and fracture behavior of Nodular Ductile Iron (NDI) and its underlying ferritic matrix phase, primarily focusing on the Johnson-Cook strength and failure models. The research involved quasistatic and split Hopkinson pressure bar (SHPB) compression tests on NDI and a Fe-Si alloy, which served as a model material for the ferritic matrix. Through these tests, the study determined various Johnson-Cook parameters, such as yield strength, strain hardening coefficients, and strain rate sensitivity, along with failure parameters specific to the NDI. The work also included the development of fracture statistics based on different specimen sizes, which are crucial for initializing simulations of fragmentation events. The study's findings contribute significantly to the understanding of NDI's mechanical properties under different loading conditions and provide essential data for continuum-scale simulations of dynamically loaded NDI components.

Salomonsson and Olofsson (2022)[6] conducted an analysis of localized plastic strain in heterogeneous cast iron microstructures using three-dimensional finite element simulations. The study captured the microstructural features of various cast irons through micro-X-ray tomography, which were then used to generate three-

dimensional finite element models. The research aimed to identify microscopic factors that could lead to fatigue crack initiation in cast iron alloys and to incorporate this knowledge into larger-scale structural simulations. The results indicated that the SGI microstructure exhibited more pronounced localized plastic strains compared to other types of cast iron. Additionally, the study emphasized that three-dimensional representations of microstructures provide more accurate predictions of strain fields than two-dimensional analyses.
Liu et al. (2020)[7] conducted an extensive study on the dynamic behavior and damage characteristics of GJS-450 cast iron under varying strain rates. The researchers performed uni-axial quasi-static and dynamic tensile tests at strain rates ranging from 10^{-4} to 250 s^{-1} , utilizing specimens with different geometries to capture the stress-strain curves and fracture strains of the material. The study introduced a strain rate-dependent plastic flow law based on the Voce model to describe the mechanical behavior of GJS-450 in this strain rate range. Moreover, the existing Bai-Wierzbicki damage model was extended to account for strain rate effects, and the modified models were calibrated using local fracture strain data. The proposed constitutive and damage models were validated through simulations, which showed excellent agreement with experimental results. The study highlights the nonlinear effects of strain rate on the yield stress and fracture strain of GJS-450, demonstrating the applicability of the extended models for predicting the mechanical behavior of cast iron alloys under dynamic loading conditions.

Memhard et al. (2011)[8] developed a material model aimed at predicting the containment safety of turbochargers under high dynamic loading and elevated temperatures. The study focused on the cast iron alloy EN-GJS-400 with nodular graphite, examining its mechanical behavior under various loading conditions, including uniaxial and multiaxial tension, compression, and shear. The researchers characterized the material's deformation and damage behaviors and incorporated these findings into a Johnson-Cook type model, along with an extended failure model to account for different failure mechanisms. The developed material model was validated through numerical simulations of penetration tests and a turbocharger containment test, showing good agreement with experimental data. This model provides a critical tool for reducing the cost and complexity of safety testing in turbocharger development by enabling accurate simulations of material behavior under extreme conditions.

In the literature, various test methods have been employed for different cast iron materials to obtain Johnson-Cook (JC) damage and material models, while in some cases, only the material model has been derived. In certain studies, the obtained parameters were input into finite element-based software to compare the results with experimental data, whereas in others, only the material parameters were determined. Additionally, in some of the studies, the microstructure was examined to investigate its influence on the material properties.

With the advancement of technology, the use of computer software in solving engineering problems has steadily increased. One of the methods employed by these software programs, the Finite Element Method (FEM), is widely used for modeling problems related to statics, strength, fatigue, ballistics, machining, fracture mechanics, and heat transfer. Among the many parameters that must be carefully considered to ensure that the results obtained from these software programs are realistic, one of the most crucial is the selection of an appropriate material and damage model to accurately simulate the mechanical behavior of the material. In this study, the aim is to obtain the Johnson-Cook material and damage parameters for the GJS-400 nodular cast iron and to compare the material parameters obtained with real test data using finite element software.

2. Material and Method

In this section, the properties of the materials used and the methods used within the scope of the study will be explained.

2.1. Material

In this study, EN-GJS-400 nodular cast iron material was used. A spectral analysis was conducted to determine the proportions of the alloying elements, and the alloy composition is presented in Table 1. Microstructural images were captured to identify the microstructure of the material, and these are shown in Figure 1.

Table 1. Nominal composition of EN-GJS-400 Cast Iron %

C	Si	Mn	P	S	Cr	Cu
4,23	2,68	0,170	0,0162	0,0089	0,0318	0,110

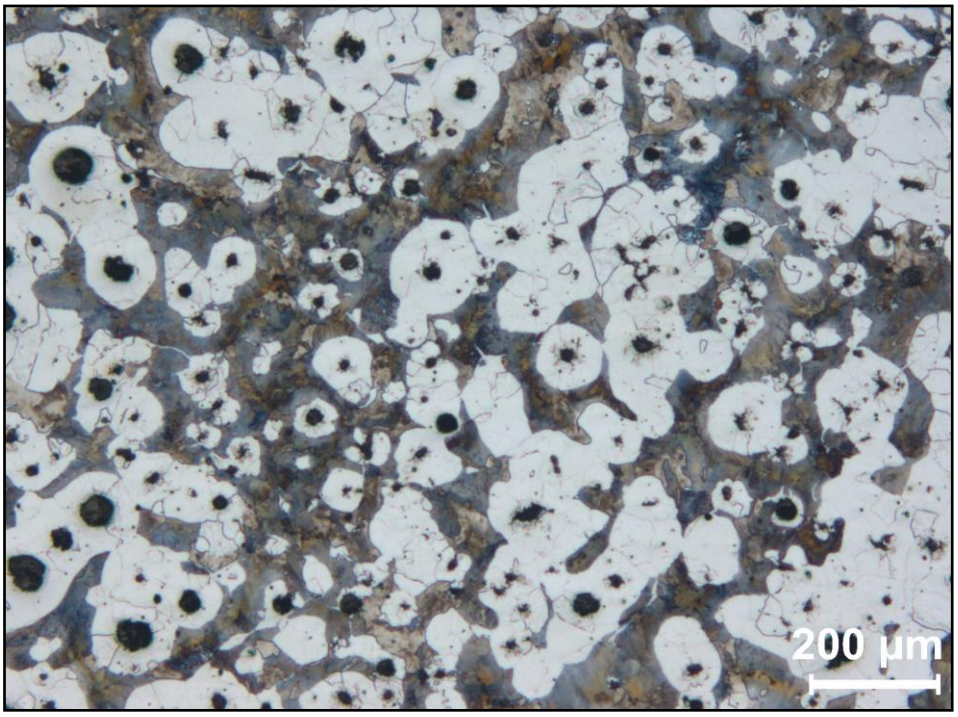

Figure 1. Microstructure of EN-GJS-400.

The technical drawings of the specimens used in the tensile, compression, and Split Hopkinson tests are presented in Figures 2, 3, and 4, respectively.

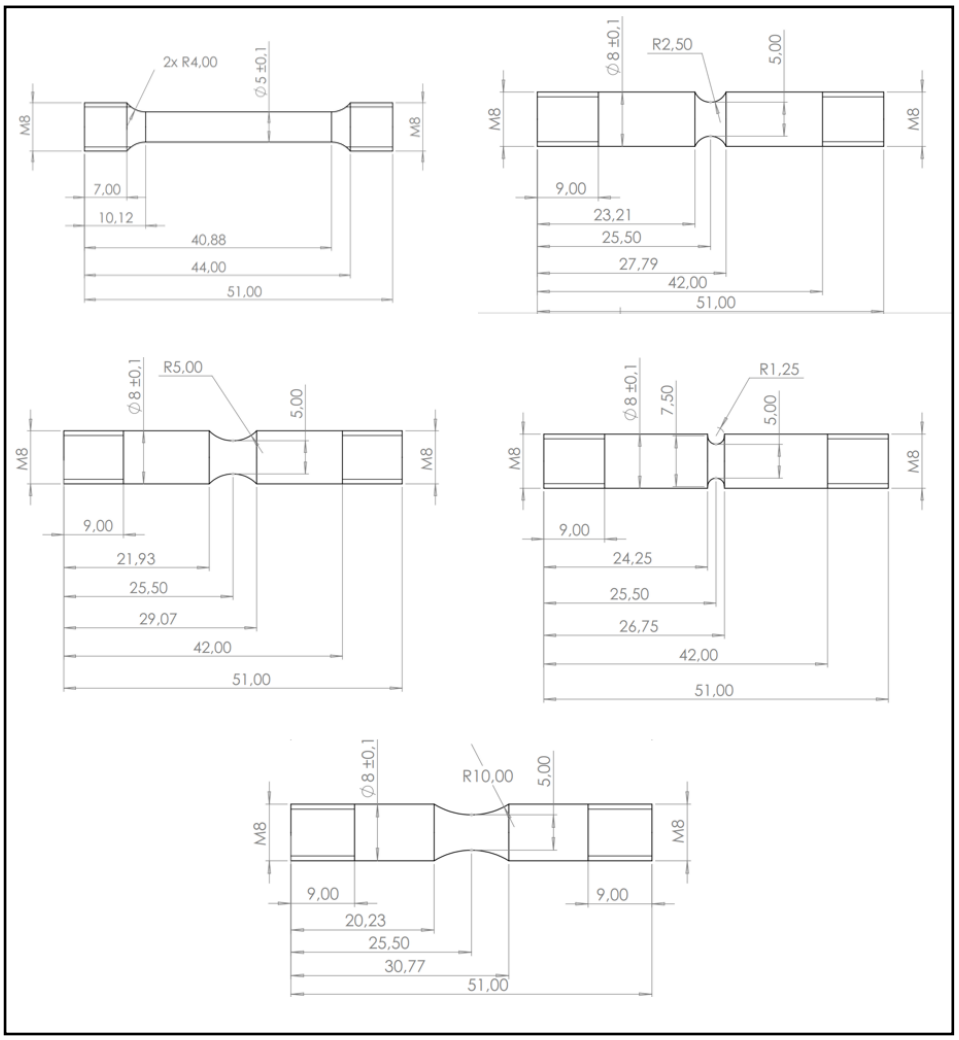

Figure 2. Geometry and dimensions of tensile specimens.

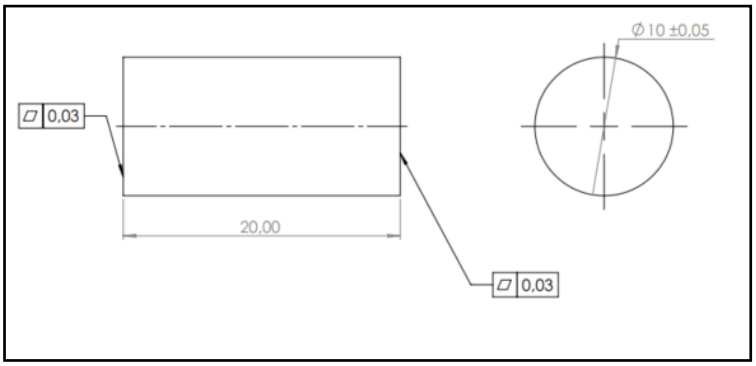

Figure 3. Geometry and dimensions of compressive specimens.

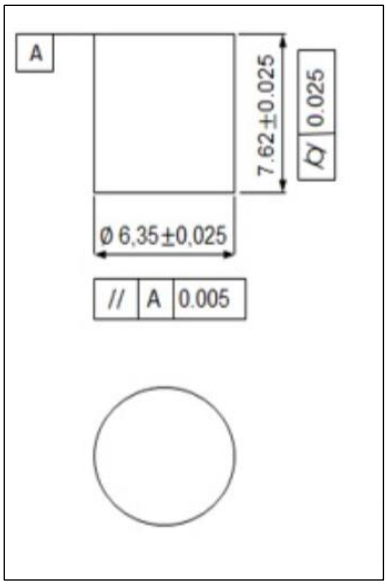

Figure 4. Geometry and dimensions of SHPB specimens.

2.2. Methods

In this section, the methods used will be explained.

2.2.1. Low Strain Rate Experiments

The tensile tests were conducted according to TS EN ISO 6892-1: Method B, with a strain rate of 0.011/s, and the compression tests were performed at tensile and compression speeds of 0.01 mm/s using an MTS Criterion 43 model servo test machine under room conditions. To ensure the repeatability of the experiments, at least three tests were performed for each specimen.

2.2.2. High Strain Rate Experiments

Dynamic compression tests were conducted at four different strain rates under room conditions. The experiments were performed using a Rel brand Split Hopkinson Pressure Bar (SHPB) test setup. Although the strain rates were not identical for each specimen, they were approximately 1100, 2300, 4075, and 5470/s. To ensure the repeatability of the experiments, at least two tests were conducted at each strain rate. A schematic representation of the SHPB test setup is provided in Figure 5.

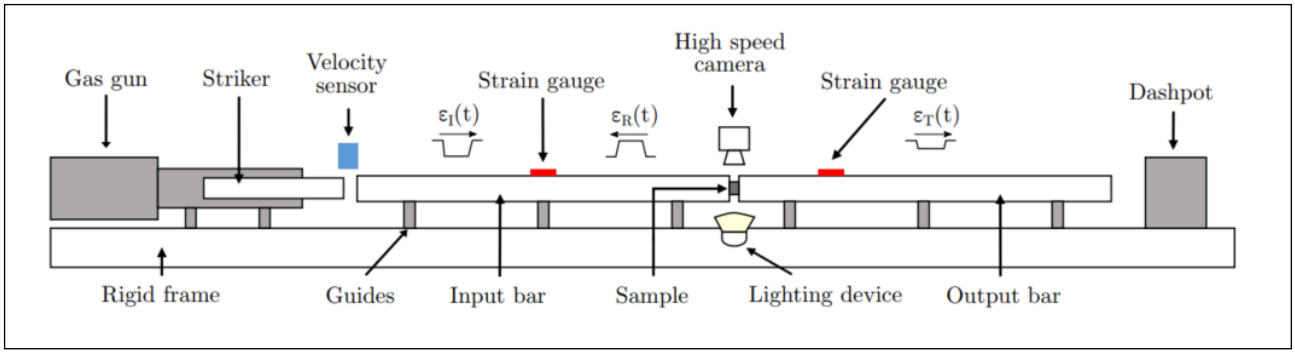

Figure 5. SHPB test schematic.

2.2.3. High Temperature Experiments

High-temperature tensile tests were conducted using an INSTRON 8852 model servo test machine at temperatures of 300°C, 500°C, and 700°C. To ensure the repeatability of the experiments, at least two tests were performed for each specimen.

2.2.3. The Johnson–Cook Material Model

This material model is one of the widely used models to obtain the flow stress of materials as a function of strain, strain rate, and temperature.[9] The flow stress model is expressed as follows:

$$\sigma = (A + B\epsilon^n)(1 + C\ln\dot{\epsilon}^*)(1 - T^{*m}) \quad (1)$$

Here, σ represents the equivalent stress, ε denotes the strain, A is the yield strength, B is the strain hardening coefficient, n is the strain hardening exponent, C is the strain rate sensitivity coefficient, and m is the stress softening exponent.

$$[\dot{\epsilon}^* = \frac{\dot{\epsilon}}{\dot{\epsilon}_0}, \quad T^* = \frac{T - T_{\text{ref}}}{T_m - T_{\text{ref}}}] \quad (2)$$

Here, $\dot{\epsilon}^*$ represents the dimensionless strain rate T* is the homologous temperature, Tm is the material's melting temperature, and T denotes the deformation temperature. $\dot{\epsilon_{\text{ref}}}$ is the reference strain rate, and T_{ref}, is the reference deformation temperature.

To calculate the material coefficients B and n, Equation 1 is rearranged under the reference strain rate and reference temperature conditions, resulting in Equation 3.

$$\sigma = A + B\epsilon^n \quad (3)$$

Taking the natural logarithm of Equation 3, it can be rewritten as shown in Equation 4.

$$\ln(\sigma - A) = \ln B + n\ln\epsilon \quad (4)$$

The value of A can be obtained from the tensile test conducted under the reference strain rate and reference temperature. By inserting the flow stress and strain data under reference deformation conditions into the equation, a linear relationship graph between $\ln(\sigma - A)$ and $\ln\epsilon$ can be constructed. By fitting the data to the equation and using a regression line approach, the material parameters B and n can be determined

$$\sigma = A + B\epsilon^n \quad (5)$$

When the deformation temperature is T=Tref, Equation (1) can be edited as shown below [19]:

$$\frac{\sigma}{(A + B\,\varepsilon^n)} = 1 + C\ln\left(\frac{\dot{\varepsilon}}{\dot{\varepsilon}^0}\right) \quad (6)$$

After determining the values of the material parameters, A, B, and n, the $\frac{\sigma}{(A + B\ \varepsilon^n)}$ - $\ln\left(\frac{\dot{\varepsilon}}{\dot{\varepsilon}^0}\right)$ curve is plotted. Linear fitting can be performed using various strain rates with a regression model. Finally, the material constant C can be calculated using the slope of the linear fitting curve.

Equation 1 can be rearranged with respect to the reference strain rate as follows:

$$\sigma = (A + B\,\epsilon^n)(1 - T^{*m}) \tag{7}$$

Taking the natural logarithm of both sides and rearranging the equation, Equation 7 can be expressed as follows:

$$\ln\left(1 - \frac{\sigma}{A + B\epsilon^n}\right) = m \ln T^* \tag{8}$$

Next, by substituting the material parameters A, B, and n into the equation above and using a regression model, we can obtain the mmm parameter from the graph of the linear fitting curve. [6].

2.2.3. The Johnson–Cook Failure Model

The Johnson-Cook failure model indicates that the fracture strain generally depends on the stress triaxiality ratio, temperature, and strain rate. [10]The Johnson-Cook failure model is shown below.

$$\epsilon_f = \left[D_1 + D_2 \exp\left(D_3\left(\frac{\sigma_m}{\sigma_{eq}}\right)\right)\right][1 + D_4 \ln(\dot{\epsilon^*})][1 + D_5 T^*] \tag{9}$$

Here, ε_f is the failure strain, D_1 is the initial failure strain, D_2 is the exponential factor, D_3 is the triaxiality factor, D_4 is the strain rate parameter, and D_5 is the temperature parameter. σ_m is the mean stress, and σ_{eq} is the equivalent stress. The ratio $\left(\frac{\sigma_m}{\sigma_{eq}}\right)$ is known as stress triaxiality.

The first bracket in the JC failure model in Equation 9 includes the failure strain, exponential factor, and triaxiality factor (D1, D2, D3) respectively. These parameters can be determined by testing unnotched and notched tensile specimens at the reference strain rate and reference temperature. Under reference strain rate and reference temperature, Equation 9 can be written as follows.

$$\epsilon_f = [D_1 + D_2 \exp(D_3 \sigma^*)) \tag{10}$$

Using the data from notched and unnotched tensile tests, a fracture strain versus stress triaxiality graph can be generated. By fitting an exponential curve to the points on this graph, the parameters D_1, D_2, and D_3 can be obtained.

The strain rate parameter D_4 in the JC failure model can be determined from the failure strains of specimens tested at different strain rates under reference temperature. At the reference temperature, Equation 9 can be expressed as follows:

$$\epsilon_f = [D_1 + D_2 \exp(D_3 \sigma^*)]\left[1 + D_4 \ln\left(\frac{\dot{\epsilon}}{\dot{\epsilon_0}}\right)\right] \tag{11}$$

When Equation 11 is rearranged, it can be written as follows:

$$\frac{\epsilon_f}{[D_1 + D_2 \exp(D_3 \sigma^*)]} - 1 = D_4 \ln\left(\frac{\dot{\epsilon}}{\dot{\epsilon_0}}\right) \tag{12}$$

Thus, the D_4 parameter can be obtained by plotting the failure strain versus logarithmic strain rate curve and applying linear curve fitting

The final parameter of the JC failure model, D_5, can be determined from the failure strains of unnotched specimens tested at different temperatures and the reference strain rate. At the reference strain rate, Equation 9 can be expressed as follows:

$$\epsilon_f = [D_1 + D_2 \exp(D_3\sigma^*)]\left[1 + D_5\left(\frac{T - T_r}{T_m - T_r}\right)\right] \quad (13)$$

When Equation 13 is rearranged, it can be written as follows:

$$\frac{\epsilon_f}{[D_1 + D_2 \exp(D_3\sigma^*)]} - 1 = D_5\left(\frac{T - T_r}{T_m - T_r}\right) \quad (14)$$

Therefore, fitting the above equation to the experimental failure strain versus temperature curve will yield the value of D_5.

2.2.4. Finite Elements Model

In this study, the Abaqus software package was used as the finite element analysis (FEA) tool. The solid model of the flat tensile test specimen used in the analysis is shown in Figure 6, and the finite element model is depicted in Figure 7. The obtained Johnson-Cook (J-C) material and failure model parameters were defined in the Abaqus software. The mesh model used linear hexahedron elements, consisting of 14,560 elements and 16,905 nodes. The boundary conditions were set by fixing one end of the specimen, while the other end was subjected to tensile loading.

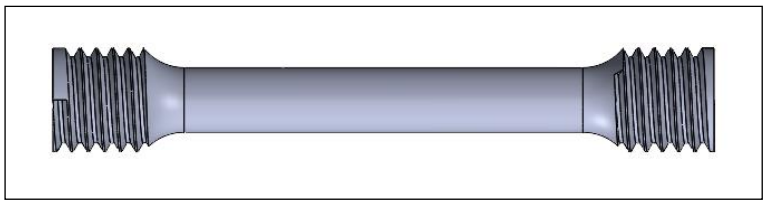

Figure 6. Tensile test specimen.

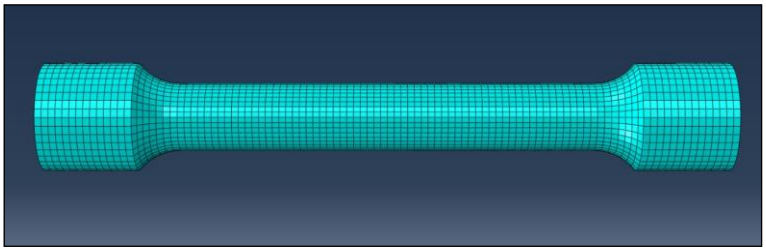

Figure 7. FE mesh model.

3. Results

3.1. Low Strain Rate Result

The results of the tensile tests conducted at room temperature and low strain rates are presented in Graph 1, while the results of the compression tests are shown in Graph 2. All stress-strain graphs provided in this study represent true stress and true strain. Upon examining both graphs, it is observed that there is no distinct yield point in the quasi-static tests; however, a noticeable strain hardening occurs during the plastic deformation phase. In the tensile tests, the strain hardening continues consistently after the yield region, whereas in the compression tests, a strain softening behavior is observed after the ultimate compressive strength. The yield strength was determined to be 310 MPa from the tensile tests and 420 MPa from the compression tests.

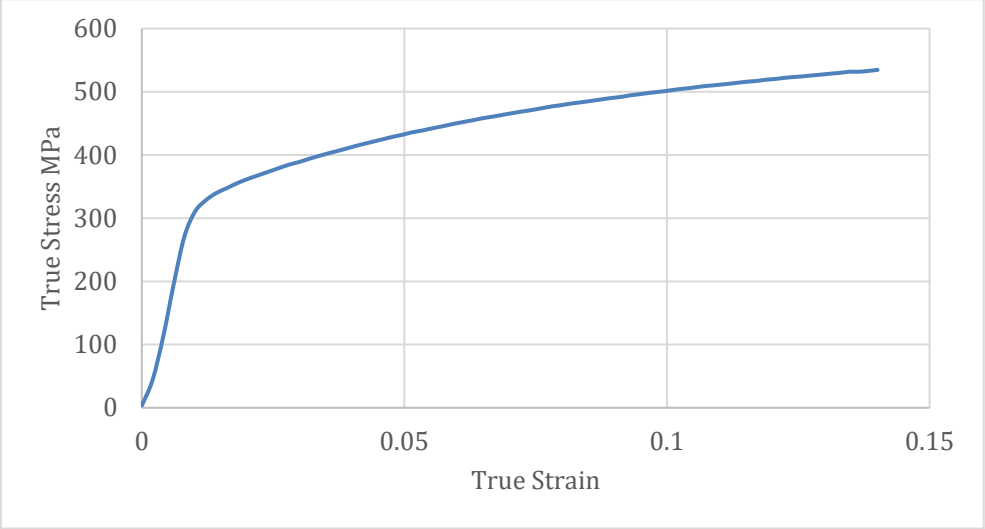

Graph 1. True Stress – True Strain curve for tensile test

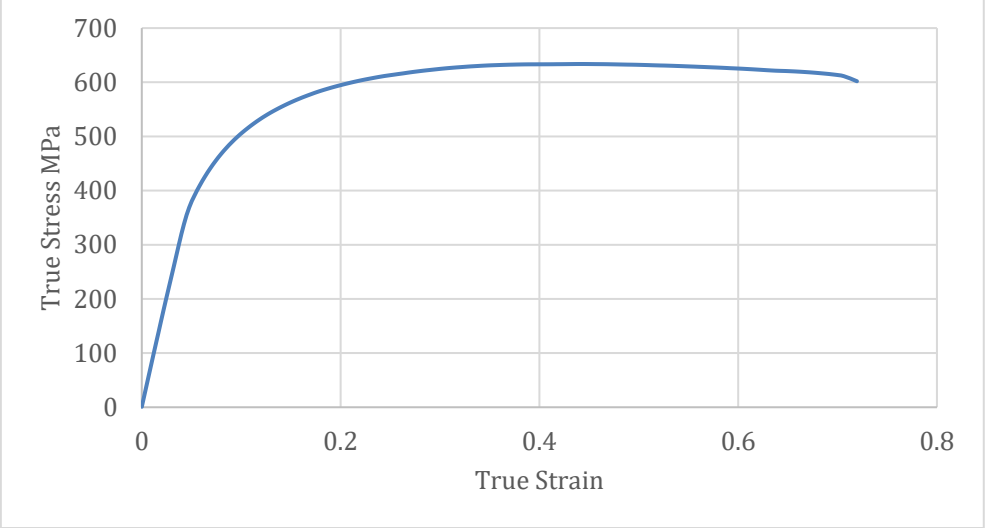

Graph 2. True Stress – True Strain curve for compressive test

The results of the notched tensile tests conducted at room temperature and low strain rates are presented in Graph 3. As the notch factor increases, the stress increases, while the strain decreases by approximately 65%.

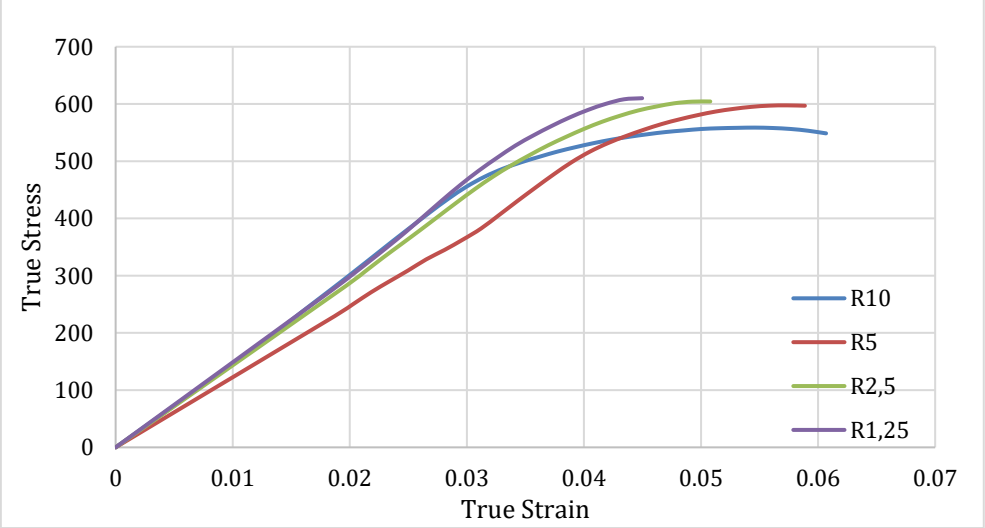

Graph 3. Fracture Strain – Stress Triaxiality for Notched Tensile Test

3.2. High Strain Rate Result

The results of the Split Hopkinson Pressure Bar tests are presented in Graph 4. The tests were conducted at room temperature with strain rates of 1103 s^{-1} 2297 s^{-1} 4074 s^{-1} and 5468 s^{-1}. While the yield point was not clearly observable in the quasi-static tensile and compression tests, it became more pronounced in the experiments conducted at high strain rates. Additionally, as the strain rate increased, the material's yield strength, ultimate tensile strength, and the amount of deformation were observed to increase.

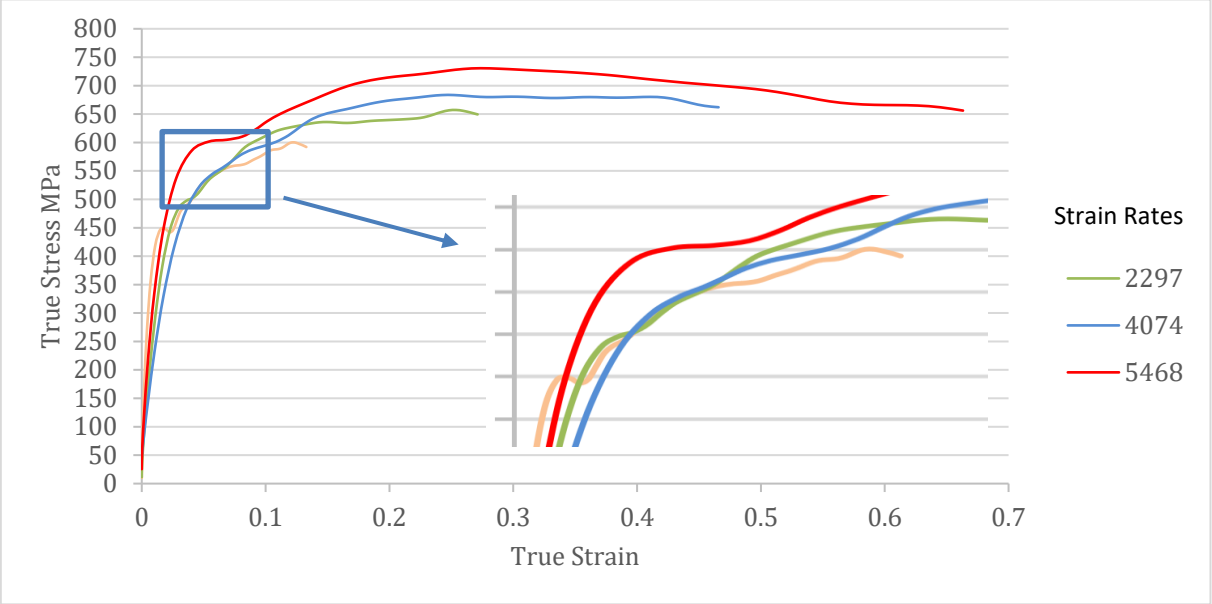

Graph 4. True Stress – True Strain curve for High Strain Rate Compressive test

3.3. High Temperature Result

The results of the hot tensile tests conducted at constant strain rates at 300, 500, and 700°C are presented in Graph 5. The experiments revealed that as the temperature increased, the material's yield strength and ultimate tensile strength decreased. In contrast to the yield and tensile strength, the amount of deformation, and therefore ductility, increased. It was also observed that with increasing temperature, the occurrence of strain hardening gradually diminished.

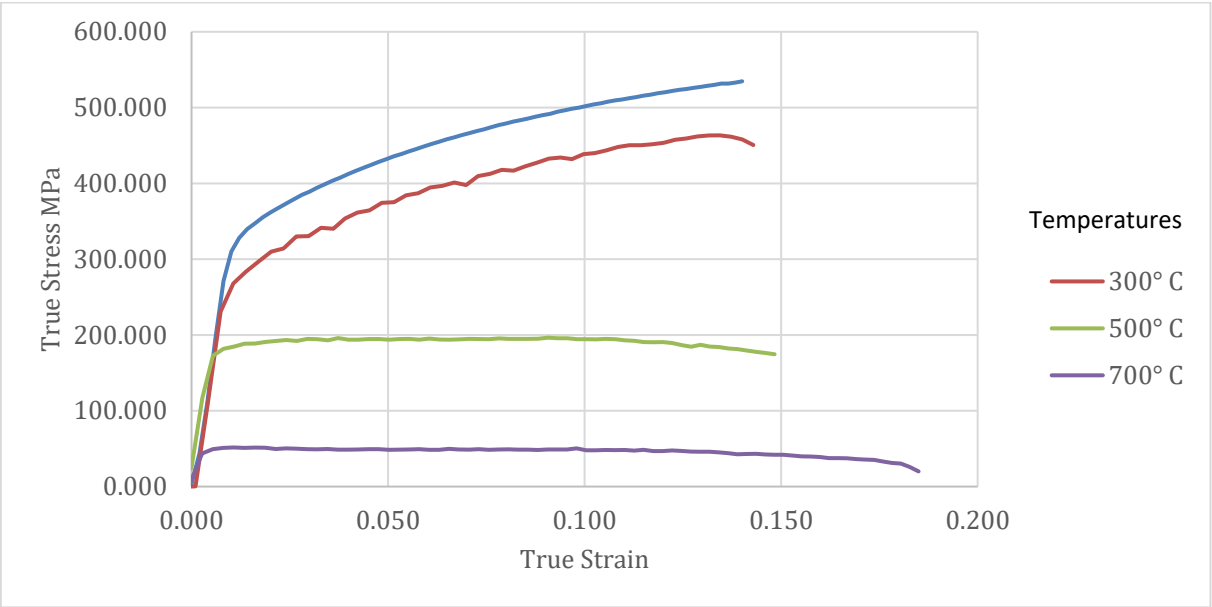

Graph 5. True Stress – True Strain curve for high temperature tensile test

3.4. The Johnson–Cook Material Model

When the data obtained from the tensile test is used with Equation 4, Graph 6 is generated, and when the data from the compression test is used, Graph 7 is obtained. The values in these graphs are fitted using the linear curve fitting method to produce a first-degree equation. The constant term of this equation provides the B coefficient as 6.5902, and the exponent of the coefficient in front of x gives the n value

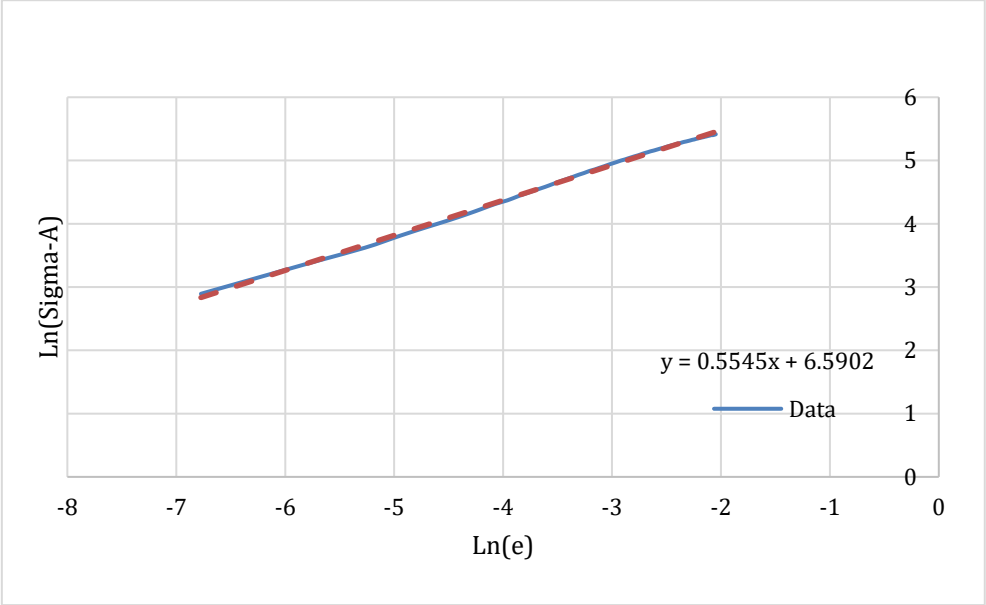

Graph 6. Ln(Sigma-A) vs Ln(e) (Tensile)

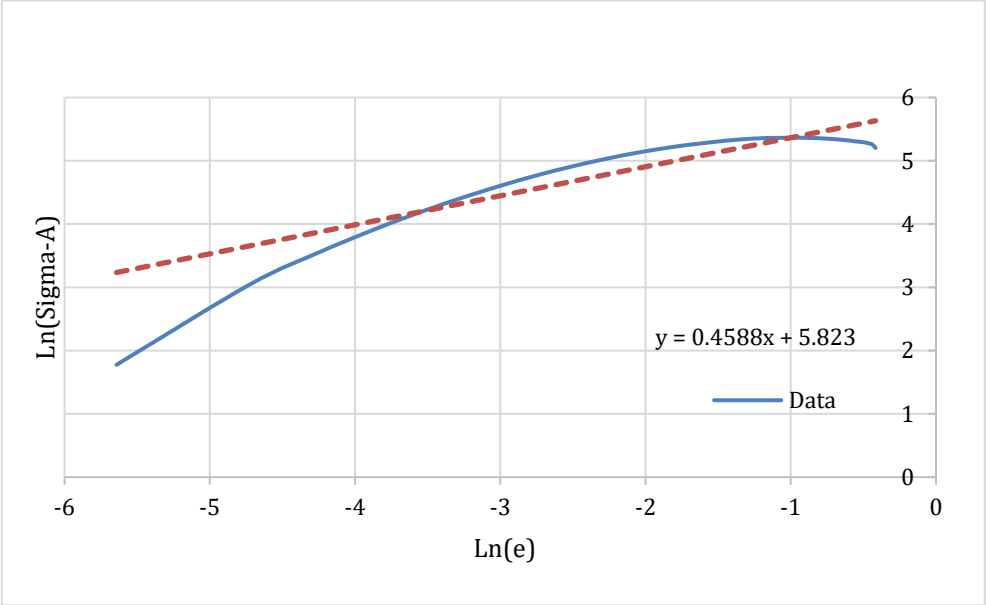

Graph 7. Ln(Sigma-A) vs Ln(e) (Compression)

In the tensile and compression tests conducted so far, the parameters A, B, and n have been determined. Using these parameters and the data obtained from the SHPB tests, Graphs 8 and 9 are generated with the help of Equation 6. The values in these graphs are fitted with a linear curve using the linear curve fitting method. The slope of this curve will provide the value of the coefficient c.

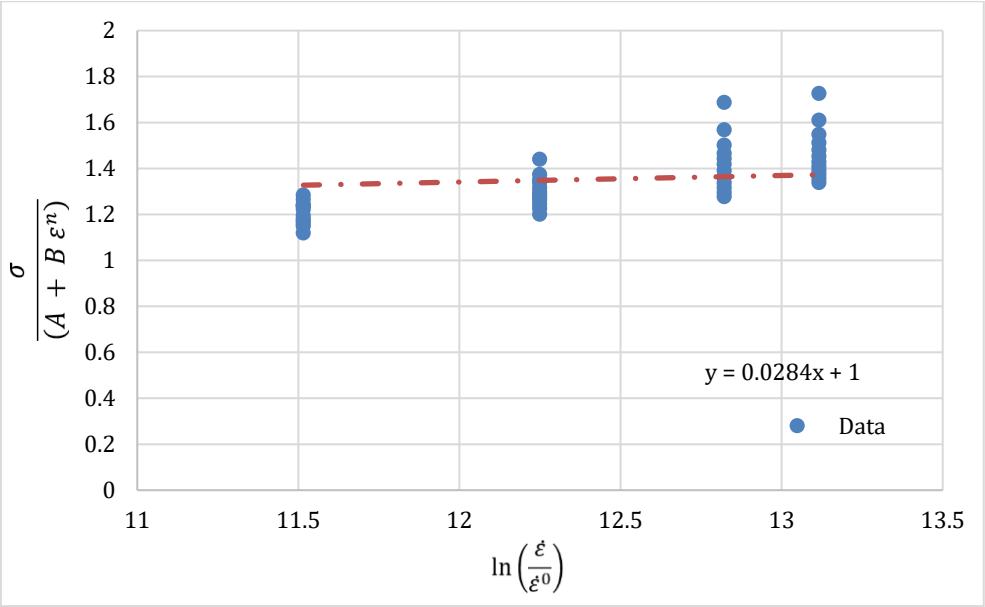

Graph 8. Relationship between Strain Rate and Normalized Stress (Linear Fitting) (Tensile)

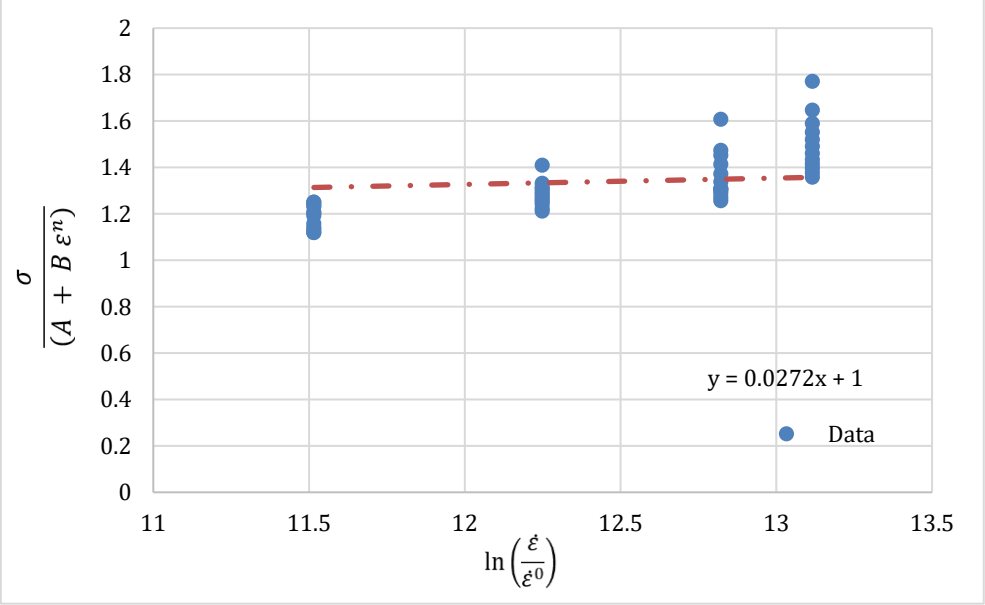

Graph 9. Relationship between Strain Rate and Normalized Stress (Linear Fitting) (Compression)

Using the results from the high-temperature tensile tests and the tensile and compressive tests conducted at room temperature, the parameters A, B, and n are applied in Equation 8 to generate Graph 10 and 11. The values in this graph are fitted using the linear curve fitting method to produce a curve. The slope of this curve provides the m coefficient.

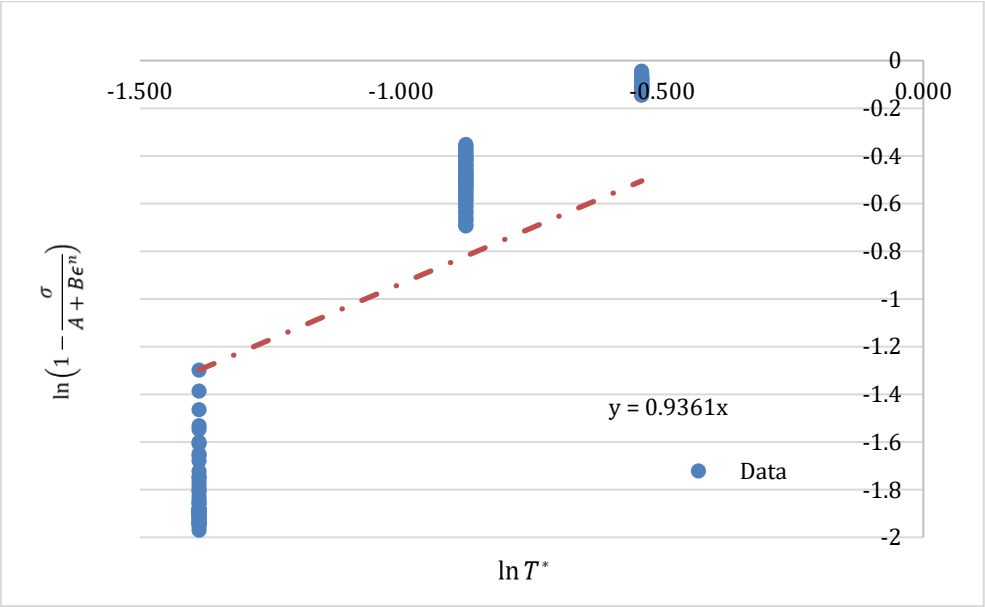

Graph 10. Relationship between $\ln\left(1-\frac{\sigma}{A+B\varepsilon^n}\right)$ and $\ln T^*$ for Tensile

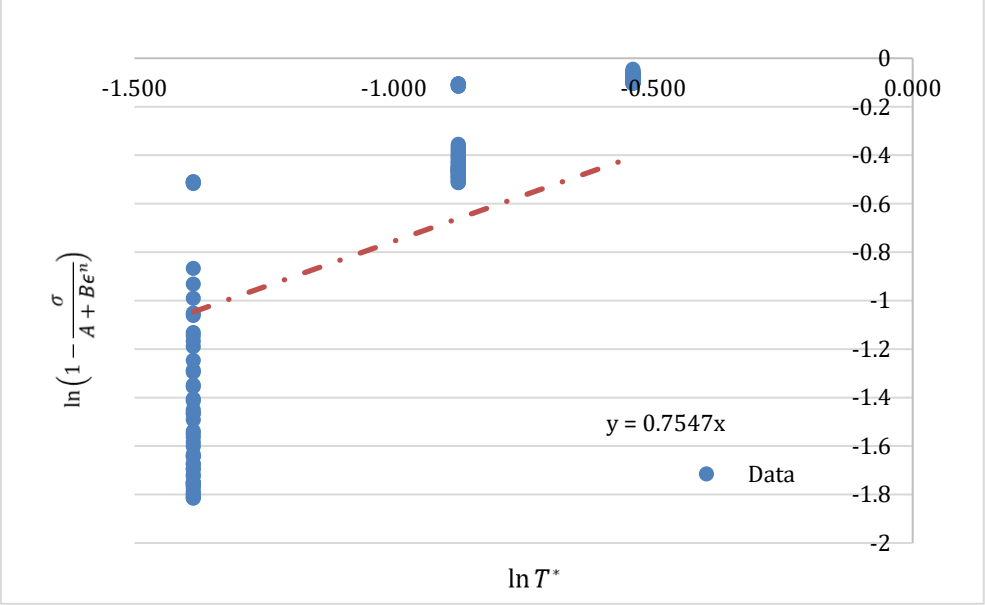

Graph 11. Relationship between $\ln\left(1-\frac{\sigma}{A+B\varepsilon^n}\right)$ and $\ln T^*$ for Compressive

A(MPa)	B(MPa)	n	C	m	
310	728	0,5545	0,0241	0,9361	A, B and n parameters were calculated using tensile test
420	338	0,459	0,0272	0,7547	A, B and n parameters were calculated using compressive test

3.4. The Johnson–Cook Failure Model

The graph of Fracture Strain versus Stress Triaxiality, obtained using the data from the notched tensile test, is presented in Graph 12. The values in this graph can be fitted using the exponential curve fitting method to derive Equation 10. As a result, the parameters D1=0.0498, D2=1.5752, and D3=−8.5926 are obtained. Using the data from the high-strain-rate SHPB tests and Equation 12, Graph 13 can be generated, from which the D4 parameter can be obtained using the linear curve fitting method. Similarly, the data from the high-temperature tensile tests and Equation 14 can be used to generate Graph 14, where the D5 parameter is obtained using the linear curve fitting method.

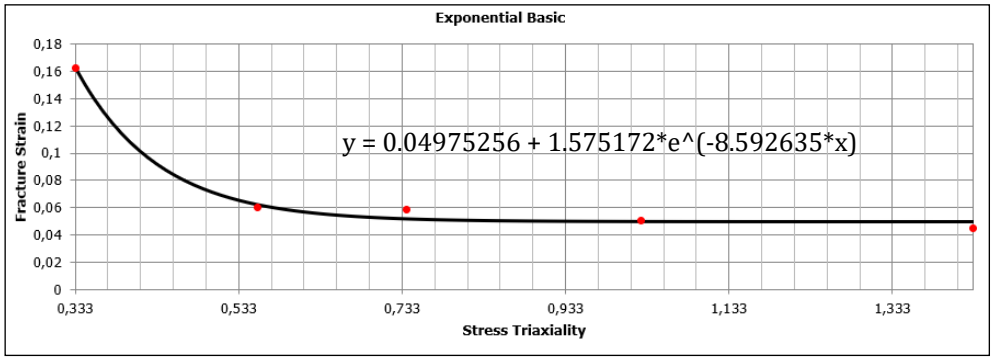

Graph 12. Fracture Strain – Stress Triaxiality for Notched Tensile Test

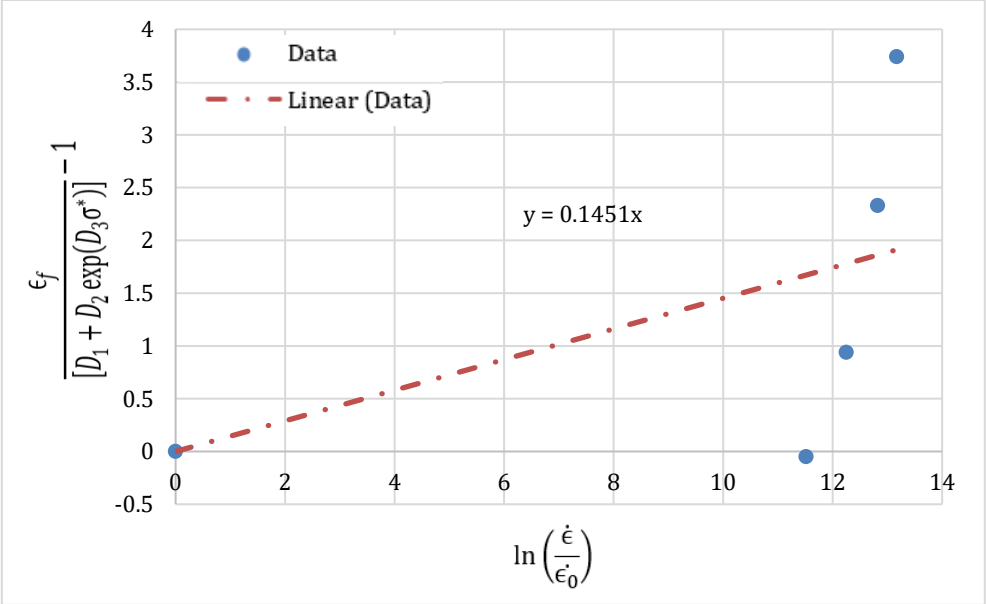

Graph 13. Relationship between $\ln\left(\frac{\dot{\varepsilon}}{\dot{\varepsilon_0}}\right)$ and $\frac{\varepsilon_f}{[D_1+D_2\exp(D_3\sigma^*)]} - 1$

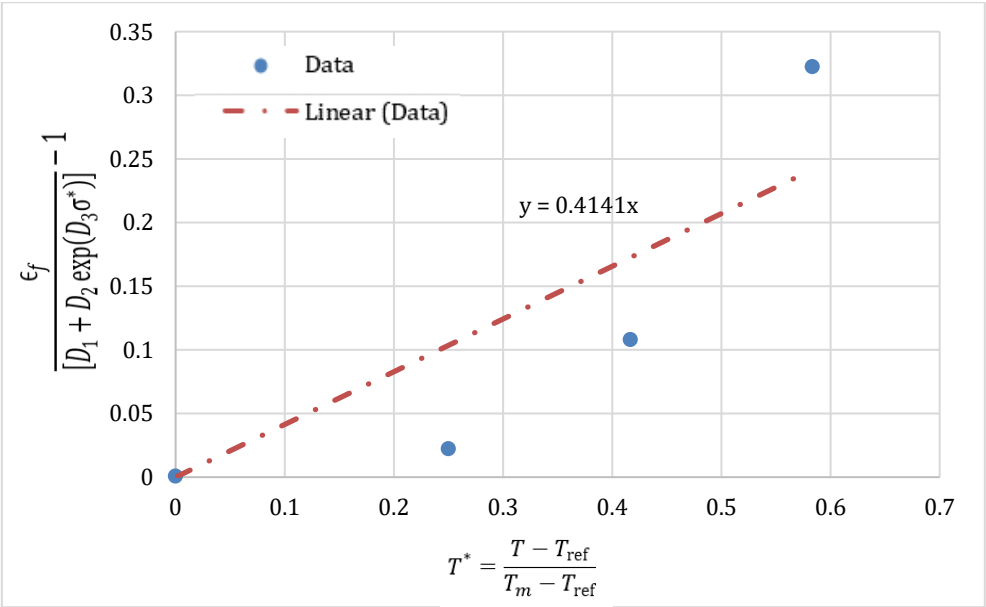

Graph 14. Relationship between $\left(\frac{T-T_r}{T_m-T_r}\right)$ *and* $\frac{\varepsilon_f}{[D_1+D_2\exp(D_3\sigma^*)]-1}$

3.5. Finite Element Analysis Result

The tensile test data obtained using the Abaqus software, along with the experimental data, are presented in Graph 15. Upon examining the results, it is observed that the finite element analysis data closely match the experimental results. The maximum difference between the two sets of results is 0.005.

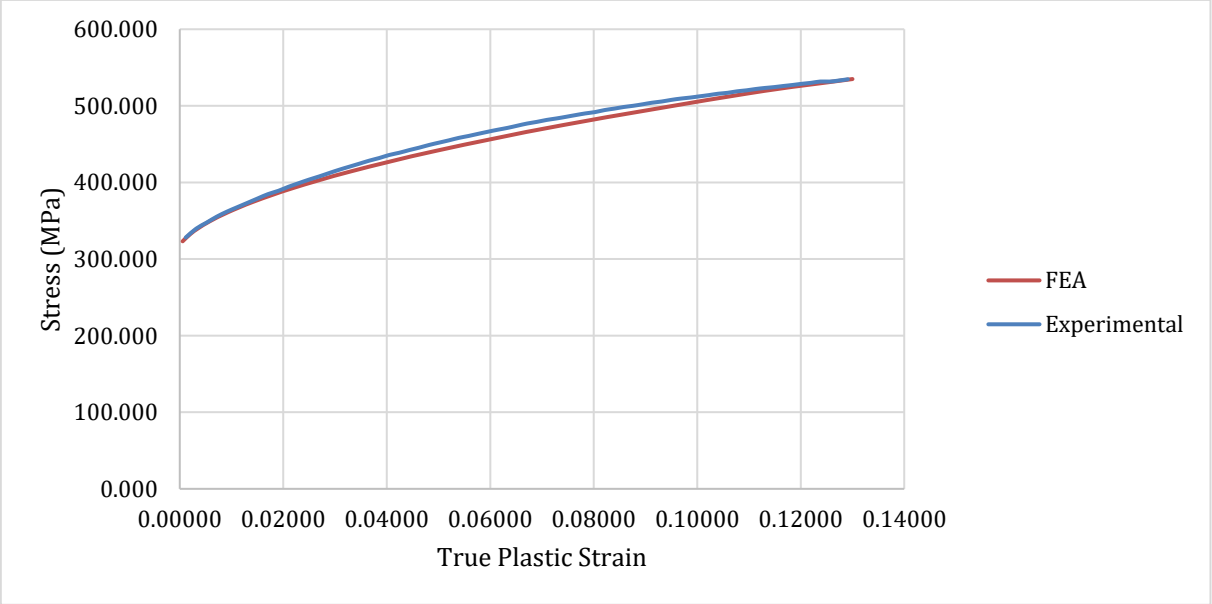

Graph 15. True Stress – True Plastic Strain curve for FEA vs Experimental (Tensile)

The compression test data obtained using finite element analysis, along with the experimental data, are presented in Graph 16. Upon examining the results, it is observed that the finite element analysis data closely match the experimental results. The maximum difference between the two sets of results is 0.063.

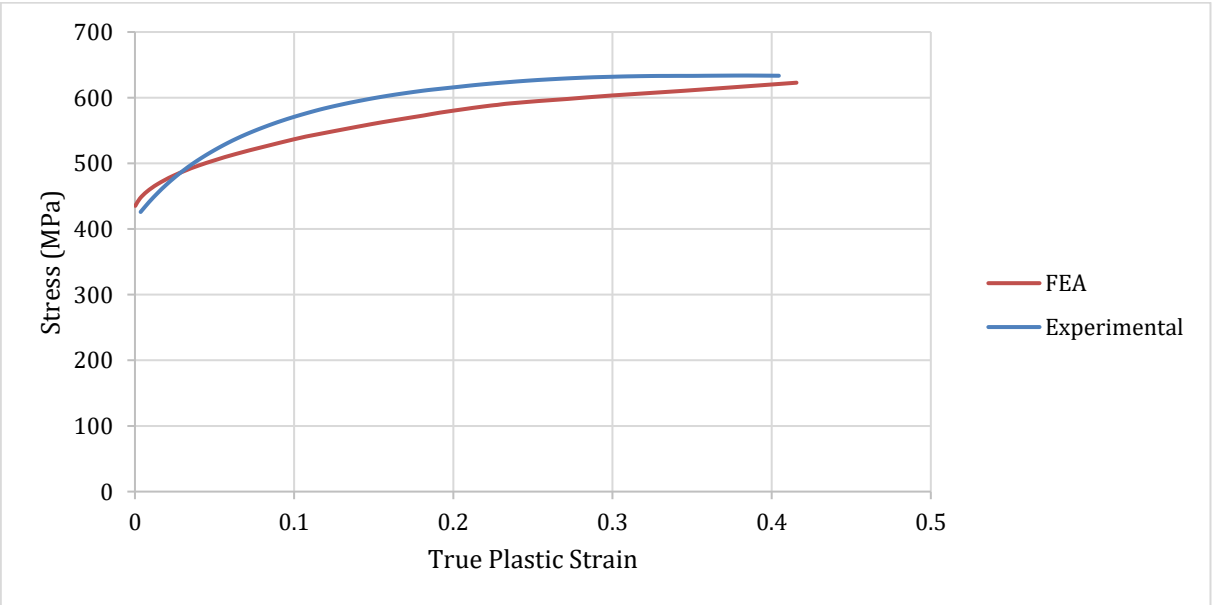

Graph 16. True Stress – True Plastic Strain curve for FEA vs Experimental (Compressive)

4. Discussion and Conclusion

In this study, the Johnson-Cook material and damage parameters for the EN-GJS-400 nodular cast iron material were comprehensively determined. The data obtained from tensile and compression tests conducted at low and high strain rates, high-temperature experiments, and Split Hopkinson Pressure Bar (SHPB) tests have provided a detailed understanding of the mechanical behavior and deformation characteristics of this material.

The Johnson-Cook material model parameters (A, B, n, C, m) and damage model parameters (D1, D2, D3, D4, D5) were calculated. These parameters were integrated into the Abaqus software for finite element analyses, and the virtual tensile and compression tests were found to be consistent with the actual test data. The tensile tests showed a difference of 0.005, while the compression tests showed a difference of 0.063.

The results of this study have helped to understand how the EN-GJS-400 material behaves under high strain rates and elevated temperatures. These findings provide valuable insights that can be used to employ the material more effectively and safely in engineering applications. Future research is recommended to investigate the effects of different cast iron types and alloying elements on such mechanical behaviors.

Acknowledgment

I would like to express my gratitude to Ekstrametal Döküm Izaba ve Mak. San. Tic. Ltd. Şti. for providing the materials used in this study, and to Assoc. Prof. Dr. MURAT AYDIN and Assoc. Prof. Dr. UMUT ÇALIŞKAN for their invaluable support during the execution of the experiments.

References

[1] Ram, N., & Gautam, V. (2022). Evaluation of Johnson-Cook material model parameters for Si-Mo-Cr ductile cast iron. *Materials Today: Proceedings, 61*, 16-20.

[2] Hellström, P., & Olander, K. (2012). *Analysis and modeling of properties of Compacted Graphite Iron on a microstructural level* (Master's thesis). Chalmers University of Technology, Gothenburg, Sweden.

[3] Ljustina, G., Larsson, R., & Fagerström, M. (2014). A FE based machining simulation methodology accounting for cast iron microstructure. *Finite Elements in Analysis and Design, 80*, 1-10.

[4] Keser, S.(2015).CGI Malzemeye Ait Malzeme Modelinin Deneysel ve AnalitikYolla Geliştirilmesi, İstanbul Teknik Üniversitesi, Fen bilimleri Enstitüsü, İstanbul.

[5] Springer, H. K. (2012). Mechanical Characterization of Nodular Ductile Iron Rep (LLNL-TR-522091). Lawrence Livermore National Laboratory.

[6] Salomonsson, K., & Olofsson, J. (2017). Analysis of localized plastic strain in heterogeneous cast iron microstructures using 3D finite element simulations. In *4th World Congress on Integrated Computational Materials Engineering (ICME 2017)* (pp. 217-225). Ypsilanti, MI, United States.

[7] Liu, C., Sun, D., Zhang, X., Andrieux, F., & Gersterc, T. (2024). Extension of flow behaviour and damage models for cast iron alloys with strain rate effect. *Chinese Journal of Mechanical Engineering, 37*(61).

[8] Memhard, D., Andrieux, F., Sun, D.-Z., & Häcker, R. (2011). Development and verification of a material model for prediction of containment safety of exhaust turbochargers. In *8th European LS-DYNA Users Conference 2011*.

[9] Johnson, G.R. and Cook, W.H. (1983) A Constitutive Model and Data for Metals Subjected to Large Strains, High Strain Rates, and High Temperatures. Proceedings 7th International Symposium on Ballistics, The Hague, 19-21 April 1983, 541-547.

[10] G. R. Johnson and W. H. Cook, “Fracture Characteristics of Three Metals Subjected to Various Strains, Strain Rates, Temperatures and Pressures,” Engineering Fracture Mechanics, Vol. 21, No. 1, 1985, pp. 31-48. http://dx.doi.org/10.1016/0013-7944(85)90052-9